Biophysical Chemistry 27 (1987) 211–224
Elsevier



BPC 01170

# Dynamic light-scattering study of muscle F-actin. II *

Satoru Fujime [a], Michiho Takasaki-Ohsita [a] and Shin'ichi Ishiwata [b]

[a] *Mitsubishi-Kasei Institute of Life Sciences, Machida, Tokyo 194,*
*and* [b] *Department of Physics, Waseda University, Shinjuku-ku, Tokyo 160, Japan*

Received 10 November 1986
Revised manuscript received 3 April 1987
Accepted 14 April 1987

Dynamic light scattering; F-Actin; Heavy meromyosin; Filament flexibility; Semidilute solution

By dynamic light scattering, the intensity autocorrelation function, $G^2(\tau) = B[1 + \beta|g^1(\tau)|^2]$, was obtained over the scattering angles ($\theta$) from 30 to 130° in steps of 10° for semidilute solutions of muscle F-actin and of F-actin complexed with heavy meromyosin in the absence of ATP (acto-HMM), where $B$ is the baseline and $\beta$ a constant. The main findings were: (1) A 0.5 mg/ml F-actin solution gave nonreproducible spectra at $\theta \leq 40°$ but quite reproducible spectra at $\theta \geq 50°$, with $\beta = 0.9$–$0.8$ at all $\theta$ values. Nonreproducibility of spectra at low $\theta$ values was concluded to be due to restricted motions of very long filaments confined in cages or zig-zag tubing formed by a major fraction of filaments, where the very long filaments were those at a distant tail of an exponential length distribution and the major fraction of filaments were those with lengths around $L_n$–$2L_n$, $L_n$ being the number-average length. Spectral widths were compared with theoretical ones for rigid rods averaged over the length distribution with $L_n = 900$ nm, and were suggested to be largely contributed at high $\theta$ values from bending motions of filaments. (2) Acto-HMM solutions at 0.5 mg/ml F-actin and at weight ratios of HMM to F-actin of 0.5–2 gave spectra which, with respect to $\theta$, behaved very similarly to those of F-actin alone. The spectral widths, however, drastically decreased with the weight ratio up to unity and stayed virtually constant above unity. In contrast to a previous study (F.D. Carlson and A.B. Fraser, J. Mol. Biol. 89 (1974) 273), $\beta$ values of acto-HMM were as large as those of F-actin alone. Acto-HMM was concluded to travel a distance far greater than $1/K$ with a mobility smaller than that of F-actin, where $K = (4\pi/\lambda)\sin(\theta/2)$, $\lambda$ being the wavelength of light in the medium. These results suggest that acto-HMM gels are very soft even though they did not pour from an inverted cell. Based on several intuitive models which give a mutual relationship between the $\beta$ value and modes of motions of scatterers, we discuss the restricted motions responsible for nonreproducibility of spectra at low angles and large $\beta$ values of acto-HMM gels at all $\theta$ values and weight ratios so far studied.

## 1. Introduction

The physicochemical properties of muscle F-actin and F-actin complexed with heavy meromyosin (HMM) have been extensively studied using various techniques. Among them, a dynamic light-scattering study of F-actin and an F-actin/HMM complex in the absence of ATP (acto-HMM) was first made by Fujime and Ishiwata [1] by using an analog spectrum analyzer, and later by Carlson and Fraser [2] who employed a digital correlator. Fujime and Ishiwata claimed that F-actin in solution underwent bending Brownian motion. Carlson and Fraser, on the other hand, claimed that there was no firm evidence for the flexibility of F-actin in solution. The flexibility of F-actin, however, has been established by various studies carried out over the period 1975–1980 (see references cited in ref. 3; see also, for a review, ref. 4), and the apparent discrepancies in experimental results on F-actin

Correspondence address: S. Fujime, Mitsubishi-Kasei Institute of Life Sciences, Machida, Tokyo 194, Japan.

* Part I [3] in this series: S. Fujime, S. Ishiwata and T. Maeda, Biophys. Chem. 20 (1984) 1.

obtained by these two groups have been discussed in ref. 3.

According to the theory of dynamic light scattering [5], the normalized intensity autocorrelation function $g^2(\tau)$ of polarized light scattered from freely diffusing particles is given by $g^2(\tau) = 1 + |g^1(\tau)|^2$, where $\tau$ is the delay time and $g^1(\tau)$ the normalized field correlation function of scattered light. By definition, $g^1(\tau)$ decays from 1 at $\tau = 0$ to zero at $\tau = \infty$, and we have $g^2(0) = 2$. The experimental $g^2(0)$, however, is smaller than 2 due to nonideality under experimental conditions; $g^2(\tau) = 1 + \beta|g^1(\tau)|^2$ with $0 < \beta < 1$. Under normal conditions of dynamic light scattering, the $\beta$ value is 0.9–0.6 depending on the sizes of the pinholes in light-collection optics and the channel width $\Delta\tau$ ($\tau = n\Delta\tau$, $n$ being the channel number of a digital correlator). For the sake of convenience in the later discussion, $g^2(\tau)$ is rewritten in an unnormalized form:

$$G^2(\tau) = B[1 + \beta|g^1(\tau)|^2] \quad (1)$$

In a digital correlation method, the baseline level $B$ is known, so that the absolute value of $\beta$ can be evaluated. On the other hand, the power spectrum $S^2(\omega)$ of the intensity of scattered light is given by the Fourier transform of eq. 1; $S^2(\omega) = B[\mathrm{dc} + \beta S^1(\omega)^* S^1(\omega)]$, where $\omega$ is the angular frequency, and dc (the direct current component) and $S^1(\omega)$ denote the Fourier transforms of 1 and $g^1(\tau)$, respectively, the asterisk representing convolution. In an analog method, the dc component and hence the $\beta$ value cannot be evaluated. Since Fujime and Ishiwata [1] measured $S^2(\omega)$ by using an analog method, they neglected the $\beta$ value for acto-HMM solutions and claimed that the filament flexibility was increased by HMM binding to F-actin. Carlson and Fraser [2] observed a vanishingly small $\beta$ value for acto-HMM solutions and claimed gelation of actin filaments. Later, Fujime et al. [3] reinvestigated the same system by using a digital method and observed a large $\beta$ value contrary to the result of Carlson et al. [2,6].

This study was motivated by the following points: in 1981, we found that highly nonreproducible profiles of $G^2(\tau)$ values at F-actin concentrations above 0.3 mg/ml resulted from the appearance of very slowly decaying components which appeared to be due to the restricted motion of long filaments in a semidilute regime [3]. In that study, however, $G^2(\tau)$ was measured only at one scattering angle $\theta$ of about 32° or $K^2 = 0.90 \times 10^{10}\,\mathrm{cm}^{-2}$ ($K$ denotes the length of the scattering vector, $K = (4\pi n/\lambda_0)\sin(\theta/2)$ where $n$ is the refractive index of solvent and $\lambda_0$ the wavelength of light in a vacuum). In 1984, we measured $G^2(\tau)$ values for a 0.5 mg/ml F-actin solution at $30° \leqq \theta \leqq 130°$ and found that the profiles at $\theta \geqq 50°$ were very reproducible as shown in this paper, although the profiles at $\theta = 30$ and 40° were indeed highly nonreproducible. Very similar behavior of $G^2(\tau)$ values was also observed for acto-HMM solutions. On the other hand, such nonreproducibility in the profiles was not observed for monodisperse suspensions of bacteriophage fd at $30° \leqq \theta \leqq 150°$ and at fd concentrations up to 6 mg/ml [7]. Since bacteriophage fd is 895 nm long and 9 nm thick, its dimensions are very close to those of F-actin; the number-average length $L_n$ of F-actin is 800–1000 nm [8]. Then, there arose the question as to why nonreproducibility in the profiles appeared in the case of F-actin; i.e., was this due to its length distribution or to some other parameter(s)? Another question arose from our analysis of the polymerization process of actin by dynamic light scattering [9]. The time evolution of $G^2(\tau)$ after initiation of polymerization was followed at $\theta = 60$ or 90°, and it was found that at the time when the polymer concentration was one-fifth of the total actin concentration, about 0.4 mg/ml F-actin, a very slowly decaying component began to appear. These two recent studies [7,9] reminded us of our measurements carried out in 1984.

## 2. Materials and methods

### 2.1. Materials

Muscle proteins were obtained from rabbit back and leg white muscle. Dry muscle was prepared using almost the same method as that of Straub [10], except that the regulatory proteins were removed before acetone treatment of myosin-extracted minced muscle [11]. G-Actin was purified

according to the method of Spudich and Watt [12] with slight modifications. To prepare F-actin, 2 mg/ml G-actin filtered through a membrane filter (pore size 50 nm; Millipore) was polymerized in a 10 mm outer diameter light-scattering cell at 20 °C in 0.1 M KCl, 1 mM $MgCl_2$, 10 mM Tris-HCl (pH 8.0) and 0.5 mM ATP. 40 min after initiation of polymerization, the actin solution was diluted to 0.5 mg/ml by adding the above solvent and stored on ice. HMM was prepared according to the method of Weeds and Pope [13] by chymotryptic digestion of myosin which had been purified as described by Szent-Györgyi [14] with slight modifications. An acto-HMM complex was obtained by adding HMM (not filtered through a membrane filter) to the above F-actin solution before dilution. This mixing procedure was performed in such a way as to obtain final concentration of 0.5 mg/ml F-actin and weight ratios of 0.5, 1, 1.5 and 2 (henceforth, 'weight ratio' refers to the weight ratio of HMM to F-actin). The mixtures were left standing at 20 °C for 30 min and stored on ice. For more details, see refs. 3 and 9. Light-scattering measurements commenced 24 h after preparation of the solutions and finished within 5 days.

### 2.2. Dynamic light scattering

The spectrometer we used was of a conventional design. A 488 nm beam from an argon ion laser (Lexel, model 95) was used as a light source. Details of the spectrometer have been described elsewhere [3]. We used a 128-channel, single-clipped digital correlator [3,15], interfaced to a minicomputer (Nova 02/30, Nippon Data General). Our correlator has 16 extra channels whose delay time starts from $128(1 + M)\Delta\tau$, where $M = 1$, 2 or 3 and $\Delta\tau$ is the channel width. $G^2(\tau)$ was measured at 10 °C and at $30° \leqq \theta \leqq 130°$ in steps of 10°. For each angle, 10 runs of measurements were made successively with a data accumulation period of 180 s/run.

$G^2(\tau)$ values are displayed in the following two types of normalized forms [3]

$$\beta\,|\,g^1(\tau)\,|^2 = \beta'\big[G^2(\tau) - B\big]/B \qquad (2)$$

$$|\,g^1{}_*(\tau)\,|^2 = \big[G^2(\tau) - F\big]/\big[G^2(\Delta\tau) - F\big] \qquad (3)$$

where $\beta' = (1 + \langle n\rangle)/(1 + k)$ ($\langle n\rangle$ being the average counts of photoelectrons during the time interval $\Delta\tau$ and $k$ the clipping level), $B = G^2(\infty)$ is the baseline level, and $F$ the average of the 16 extra channels for $M = 3$.

A cumulant expansion [16] was applied to $g^1(\tau)$ in eq. 1:

$$g^1(\tau) = \exp(-\bar{\Gamma}\tau)\big[1 + (\mu_2/2!)\tau^2 - (\mu_3/3!)\tau^3\big] \qquad (4)$$

Since the correlation function had a long tail, a multiexponential fit was also applied to $g^1(\tau)$ in eq. 1:

$$g^1(\tau) = \sum_i A_i \exp(-\Gamma_i\tau) \qquad (5)$$

where $\sum_i A_i = 1.0$. An algorithm for a least-squares multiexponential fit has been described in ref. 9.

## 3. Results

### 3.1. Profiles of correlation functions

Fig. 1 shows profiles of $G^2(\tau)$ for an 0.5 mg/ml F-actin solution at various $\theta$ values (for profiles at $\theta = 90°$, see fig. 3). Ten $G^2(\tau)$ runs measured successively at each angle are displayed in normalized forms: $\beta\,|\,g^1(\tau)\,|^2$ in the left- and $|\,g^1{}_*(\tau)\,|^2$ in the right-hand panel of each pair. At $\theta = 30$ and 40°, the profiles shown on the left differed randomly from run to run as in ref. 3. As seen from the rather good reproducibility in profiles shown in the right-hand panels, nonreproducibility in successive profiles arose mostly from different sizes of $F$. Namely, there was a very slowly decaying component(s) which could not be measured with high statistical accuracy. (This component was found not to be due to dust and/or large aggregates [3].) However, at $\theta \geqq 50°$, the profiles became reproducible; the greater the angle, the better was the reproducibility. It should be noted that the $\beta$ values were 0.9–0.8 for all $\theta$ values so far studied.

Fig. 2 shows the profiles for an acto-HMM solution of 0.5 mg/ml F-actin and 0.5 mg/ml HMM (for profiles at $\theta = 90°$, see fig.3). The profiles for solutions at other weight ratios (0.5,

1.5 and 2.0) were essentially similar to those in fig. 2 and to each other. The general trends in behavior of the profiles were very similar to those in fig. 1. Although the solution of acto-HMM at 0.5 mg/ml F-actin and weight ratios greater than unity did not pour from the inverted scattering

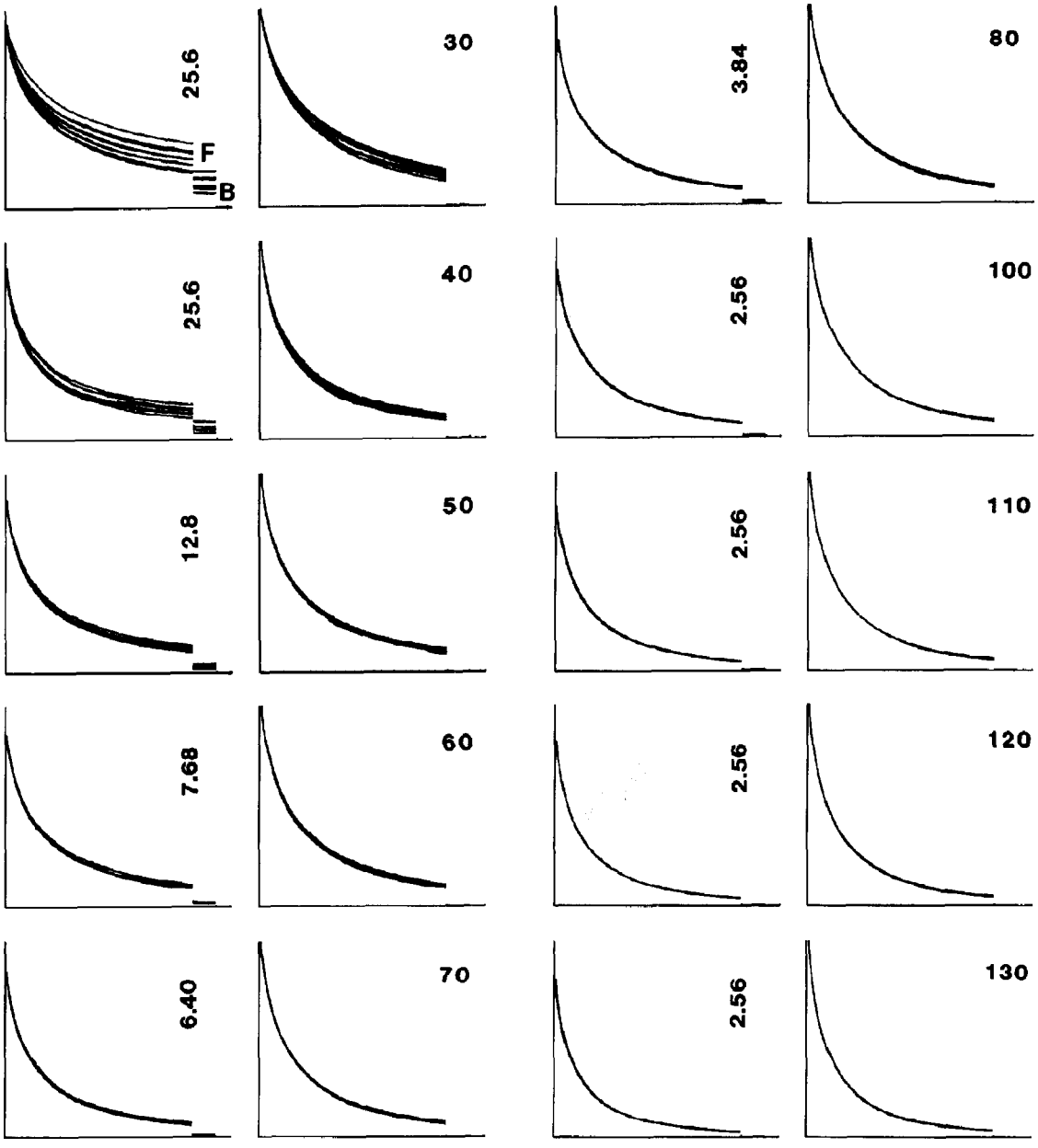


Fig. 1. Profiles of ten successively measured correlation functions in normalized forms, $\beta|g^1(\tau)|^2$ in eq. 2 on the left and $|g^1_*(\tau)|^2$ in eq. 3 in the right-hand panels in each pair. The delay time $\tau_{max} = 128\Delta\tau$ (in ms.) is given in the left panel and the scattering angle $\theta$ on the right in each pair. F and B in the top left panel denote the far-point channels and baseline, respectively. Profiles at $\theta = 90°$ are given in fig. 3. 0.5 mg/ml F-actin in 0.1 M KCl, 1 mM $MgCl_2$, 10 mM Tris-HCl (pH 8.0) and 0.5 mM ATP at 10 °C.

cell, the $\beta$ values were again 0.9–0.8 at all $\theta$ values. This contrasts markedly with the results of Carlson et al. [2,6].

Fig. 3 shows the profiles at $\theta = 90°$ for acto-HMM at 0.5 mg/ml F-actin and at weight ratios of 0, 0.5, 1, 1.5 and 2. At any weight ratio, the $\beta$

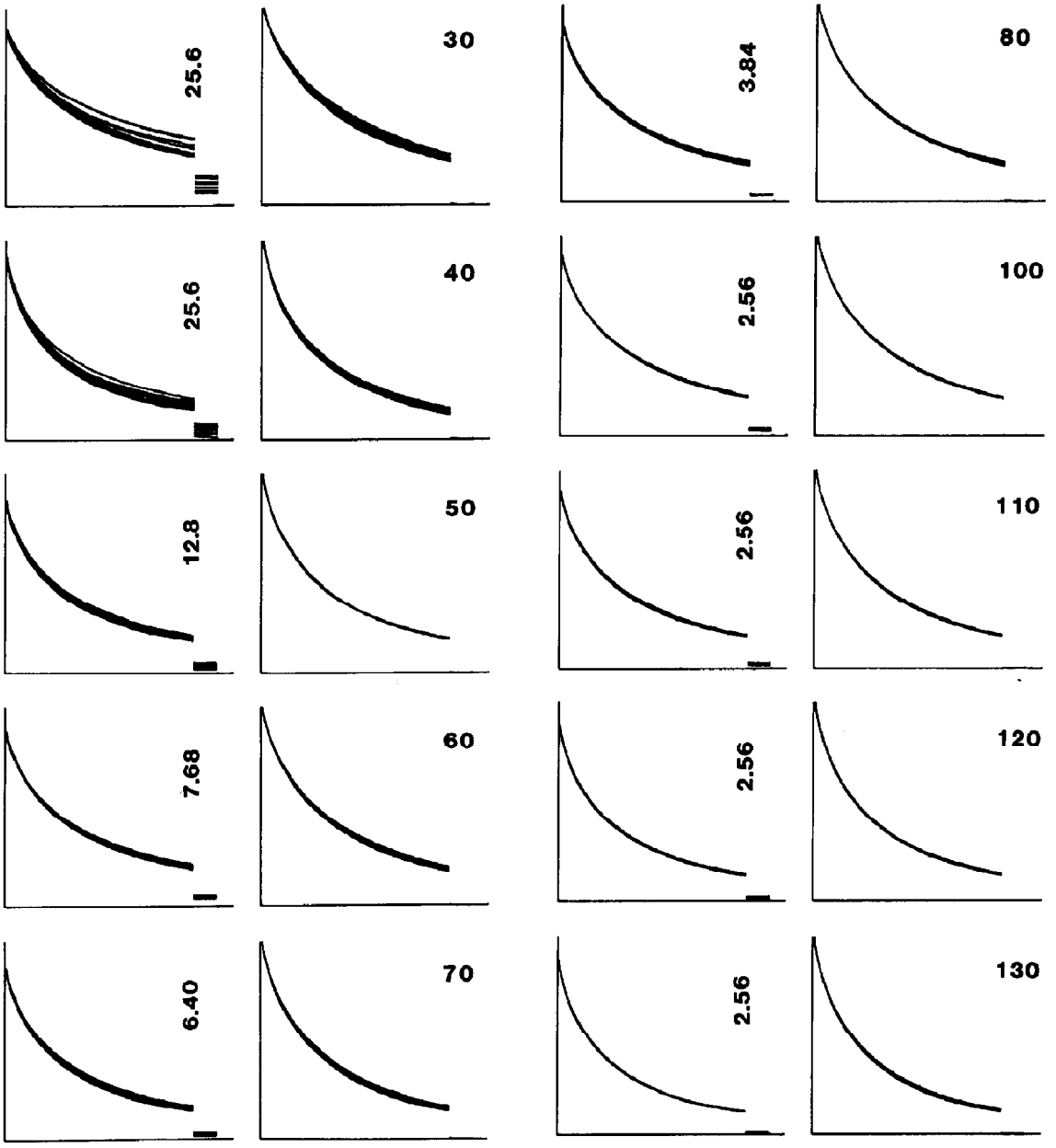


Fig. 2. Profiles of ten successively measured correlation functions in normalized forms (see legend to fig. 1). 0.5 mg/ml F-actin and 0.5 mg/ml HMM in 0.1 M KCl, 1 mM $MgCl_2$, 10 mM Tris-HCl (pH 8.0) and 0.5 mM ADP plus $P_i$ at 10 °C. (ATP in an F-actin solution had been hydrolyzed by HMM and rigor complexes of F-actin and HMM had been formed.)

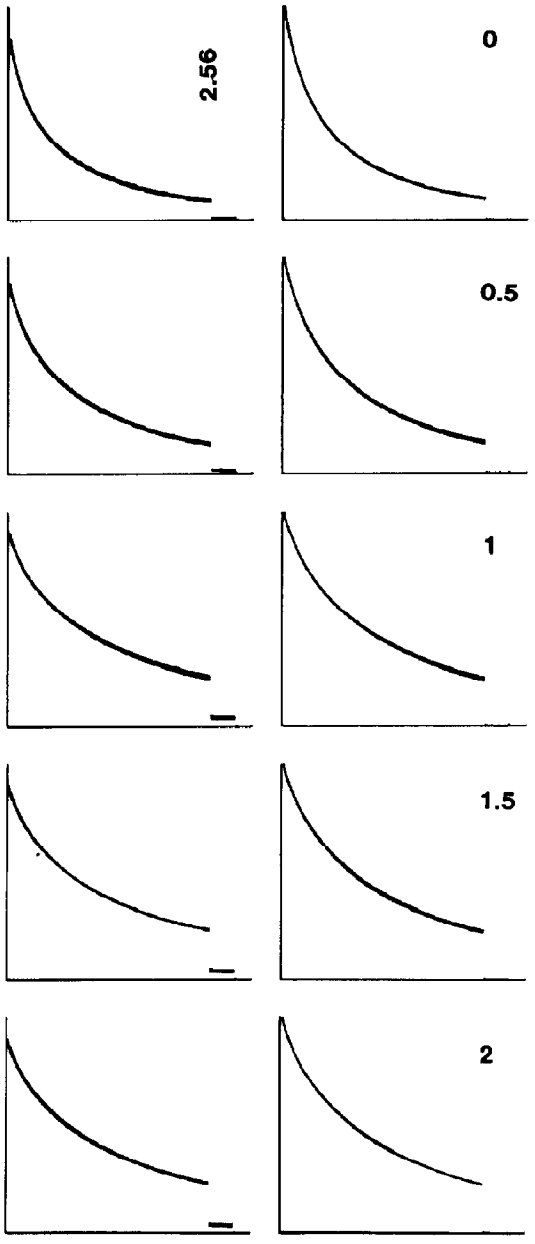


Fig. 3. Profiles of ten successively measured correlation functions at $\theta = 90°$ in normalized forms (see legend to fig. 1). 0.5 mg/ml F-actin and at weight ratios of 0–2 in 0.1 M KCl, 1 mM $MgCl_2$, 10 mM Tris-HCl (pH 8.0) and 0.5 mM ATP (ADP + $P_i$). The weight ratio is given in the top right corner of each pair. The delay time $\tau_{max} = 128\Delta\tau$ was 2.56 ms in all panels.

value was large. Comparing the profiles in fig. 3, one finds that the decay of $G^2(\tau)$ values became slower and that the $F$ value became greater as the weight ratio increased. To illustrate this feature, we made quantitative analyses of $G^2(\tau)$ values.

### 3.2. $\bar{\Gamma}/K^2$ vs. $K^2$ relationships

Fig. 4 shows the $\bar{\Gamma}/K^2$ vs. $K^2$ relationships of $G^2(\tau)$ values obtained by the third-order cumulant expansion, eq. 4. The behavior of $\bar{\Gamma}/K^2$ with respect to $K^2$ was not smooth. This resulted mainly from the fact that the value of $g^1(128\Delta\tau)$ was different from angle to angle (see figs. 1–3). The cumulant expansion did not give a good fit to the experimental $G^2(\tau)$ for short delay times,

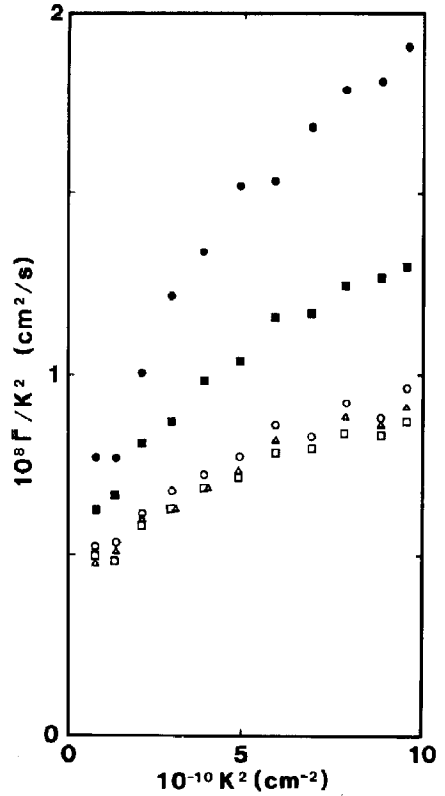


Fig. 4. The $\bar{\Gamma}/K^2$ vs. $K^2$ relationships at 10 °C obtained by third-order cumulant expansion of correlation functions for solutions of F-actin/HMM complexes at 0.5 mg/ml F-actin and at weight ratios of HMM/F-actin of 0 (●), 0.5 (■), 1 (○), 1.5 (△) and 2 (□). For solvent conditions, see legend to fig. 3.

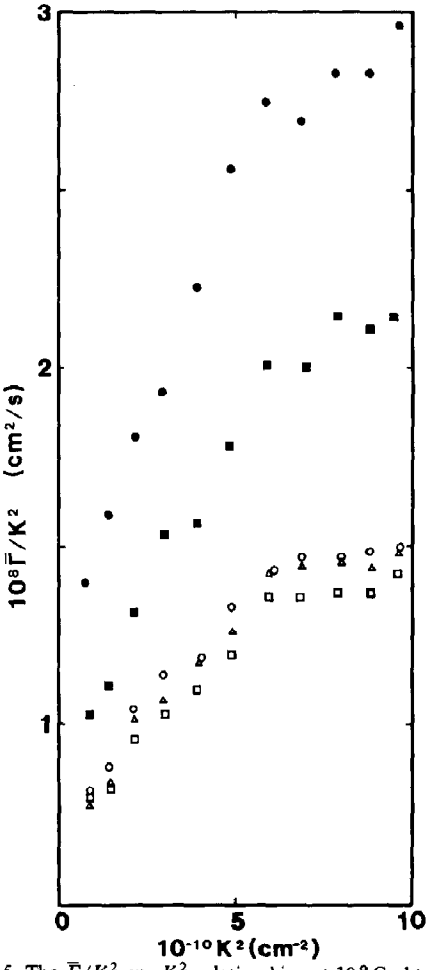


Fig. 5. The $\bar{\Gamma}/K^2$ vs. $K^2$ relationships at 10 °C obtained by three-exponential analysis (for symbols, see legend to fig. 4).

although a larger weight, $w_n = |g^1(n\Delta\tau)|^2$, was imposed for small $n$ than for large $n$ in a least-squares fit. Namely, the experimental $G^2(\tau)$ values at all $\theta$ values were highly nonexponential and also included a very fast component(s) which cannot be fitted well with the third-order cumulant expansion. The results in fig. 4 then underestimate the $\bar{\Gamma}/K^2$ values.

In order to obtain more precise fitting than in cumulant expansion, a three exponential analysis (eq. 5) was applied and the initial decay rate $\bar{\Gamma}$ was evaluated with

$$\bar{\Gamma}/K^2 = (A_1\Gamma_1 + A_2\Gamma_2 + A_3\Gamma_3)/K^2 \qquad (6)$$

Fig. 5 shows the results of the three-exponential analysis with an equal weight of $w_n = 1$. Because of better fitting over the entire delay time, the $\bar{\Gamma}/K^2$ values in fig. 5 are larger than the corresponding values in fig. 4.

## 4. Discussion

We first consider very simple but intuitive models in order to establish a mutual relationship between magnitude of the $\beta$ values and modes of motions of scatterers in dynamic light scattering. Let $N$ be the number of identical particles (spherical in shape for simplicity) in the scattering volume.

### *4.1. Model consideration*

#### *4.1.1. Model 1*

Let us assume that $pN$ particles diffuse freely and that $(1-p)N$ particles do not move relative to the laboratory-fixed coordinate system. Since the field correlation function for freely diffusing particles is given by $g_s(\tau) = \exp(-DK^2\tau)$, $D$ being the translational diffusion coefficient of the particle, the field correlation function for the total system is given by $g(\tau) = i_o + i_s g_s(\tau)$ with $i_o + i_s = 1$, from which we define

$$i_o = g(\infty),\ i_s = 1 - g(\infty),$$
$$g_s(\tau) = [g(\tau) - g(\infty)]/i_s \qquad (7)$$

Insertion of these equations into the heterodyne formula [17], $g^2(\tau) = i_o^2 + 2i_o i_s[1 + \alpha g_s(\tau)] + i_s^2[1 + \beta g_s(\tau)^2]$, gives with $\alpha = \beta$;

$$g^2(\tau) = 1 + \beta_c |g^1(\tau)|^2 \qquad (8)$$

$$\beta_c = \beta\left[1 - g(\infty)^2\right] \qquad (9)$$

$$|g^1(\tau)|^2 = \left[g(\tau)^2 - g(\infty)^2\right]/\left[1 - g(\infty)^2\right] \qquad (9')$$

Since this $|g^1(\tau)|^2$ decays to zero at $\tau = \infty$, eq. 8 has the same form as eq. 1 for $G^2(\tau)/B$, but $\beta_c$ is smaller than $\beta$ by a factor of $[1 - g(\infty)^2]$, which decreases as $i_o = g(\infty)$ increases (as $pN$ becomes smaller).

*4.1.2. Model 2*

Let $(1-p)N$ particles in model 1 have the diffusion coefficient $D_c$ ($\ll D$ for $pN$ particles), the field correlation function is given by

$$g(\tau) = i_o \exp(-D_c K^2 \tau) + i_s \exp(-DK^2\tau) \quad (10)$$

with $i_o + i_s = 1$. Since $g(\infty) = 0$, eq. 10 gives eq. 8 with $\beta_c = \beta$ irrespective of the size of positive $D_c$. When $D_c$ is extremely small, however, a very long time is needed to obtain $g^2(\tau)$ with high statistical accuracy. (This model is only a simplified one for a mixture of two kinds of scatterers with equal scattering power and different mobilities.)

*4.1.3. Model 3*

Each particle is assumed to be confined in a small compartment which does not move relative to the laboratory-fixed coordinate system. This is approximated by the situation where each particle is harmonically bound to the center of the compartment, i.e., $\zeta(dx/dt) = -\kappa x + f(t)$, where $\zeta$ is the friction constant, $x$ the position of the particle, $\kappa$ the force constant to restore the deviation $x$ and $f(t)$ the random force acting on the particle. For motion in a viscous medium, the inertia term is negligible. Under the usual assumption, $\langle x(t)f(t')\rangle = 0$ [18], we easily have $\langle x(t)x(t')\rangle = \langle x^2\rangle \exp(-\sigma\tau)$ with $\tau = |t-t'|$, $(\kappa/2)\langle x^2\rangle = k_B T/2$ and $\sigma = \kappa/\zeta$, where $\langle \ldots \rangle$ denotes the statistical average. Since $g(\tau) = \langle \exp[iK_x\{x(t) - x(t')\}]\rangle^3$, where the superscript 3 indicates taking the three components, $K_x\{x(t)-x(t')\}$, $K_y\{y(t) - y(t')\}$ and $K_z\{z(t) - z(t')\}$, and since $\langle \exp[iz(\tau)]\rangle = \exp(-\langle z(\tau)^2\rangle/2)$ for a Gaussian random variable $z(\tau) = K_x\{x(t) - x(t')\}$, we have

$$g(\tau) = \exp\left[-K^2\langle x\rangle^2\{1 - \exp(-\sigma\tau)\}\right] \quad (11)$$

This $g(\tau)$ decays to $\exp(-K^2\langle x^2\rangle) > 0$ at $\tau = \infty$. If we define $g(\tau) = i_o + i_s g_s(\tau)$ as in eq. 7, we again have eq. 8. In model 3, $\beta_c$ diminishes as $K^2\langle x^2\rangle = K^2(k_B T/\kappa)$ decreases. The square root of $\langle x^2\rangle$ is a measure of the size of the compartment which confines the particle therein. The factor $\exp(-K^2\langle x^2\rangle)$ bears analogy to the Debye-Waller factor in diffraction crystallography [19]. Since $\sigma = (k_B T/\zeta)/\langle x^2\rangle = DK^2/(K^2\langle x^2\rangle)$, we have $g(\tau) \to \exp(-DK^2\tau)$ in the limit of very large $K^2\langle x^2\rangle$, and hence $\beta_c = \beta$.

*4.1.4. Model 4*

If each compartment assumed in model 3 can diffuse through the scattering volume with a diffusion coefficient $D_c$, we have from eq. 11

$$g(\tau) = \exp(-D_c K^2\tau) \times \exp\left[-K^2\langle x^2\rangle\{1 - \exp(-\sigma\tau)\}\right] \quad (12)$$

Since $g(\infty) = 0$, eq. 12 gives eq. 8 with $\beta_c = \beta$ irrespective of the size of positive $D_c$. Note that $g(\tau)$ tends toward $\exp[-(D_c + D)K^2\tau]$ for $\tau \ll \sigma^{-1}$ and toward $\exp(-D_c K^2\tau)$ for $\tau \gg \sigma^{-1}$.

To sum up, the $\beta$ value is small when $g(\infty) \neq 0$. Bearing in mind that the above models are applicable to our problems only conceptually, we now discuss various aspects of spectra for F-actin and acto-HMM.

*4.2. F-Actin*

*4.2.1. $\beta$ value*

The $\beta$ value for F-actin alone is large in ref. 3 and in figs. 1 and 3 as well as in refs. 2 and 6, although the viscoelastic properties of F-actin solutions depend strongly on the shear rate [20], suggesting entanglement of long filaments. Entanglement will cause a restriction on the motion of filaments. Because of large $\beta$ values, the restricted motions of filaments are neither those in model 1 nor model 3 with small $\langle x^2\rangle$ but either those in models 2 and 4 with small $D_c$ or those in models 3 and 4 with large $\langle x^2\rangle$.

*4.2.2. Profiles of correlation functions*

Concerning the nonreproducibility of the profiles at low $\theta$ values, we proposed the restricted motion of long filaments in semidilute solutions of F-actin [3]. Let $L$ be the length of the filament and $c$, $c_p$ and $c^*$ be the number, mg/ml and overlap concentrations of filaments, respectively. It is evident that $cL^3 = c_p/c^*$ where $c^* = M_r/NL^3$ in units of mg/ml ($M_r$, molecular weight; $N$, Avogadro's number). Since F-actin has an exponential length distribution $N(L)$, we have the relationship $L_w = 2L_n$ where $L_n$ and $L_w$ are, re-

spectively, the number- and weight-average lengths. Since the $M_r$ of G-actin is $4.2 \times 10^7$ mg/mol and F-actin of length 1 $\mu$m has 400 G-actin, we have $M_r(L) = 16.8 \times 10^{13} \times L$ mg/mol and $\langle cL^3 \rangle = (c_p/2.8) \times 10^{10} \times \langle L^2 \rangle$. Since $\langle L^2 \rangle = 2L_n^2$, we have $\langle cL^3 \rangle = 29$ for $c_p = 0.5$ mg/ml F-actin with $L_n = 900$ nm [8]. The free volume occupied by one rod is equal to $1/c$, so that we have a cage radius of $a_c \sim L/(cL^3)^{1/2}$ [21,22]. For $L_n = 900$ nm and $\langle cL^3 \rangle = 29$, we have $a_c = 170$ nm, which should be compared with $1/K = 40$ nm at $\theta = 90°$ and 110 nm at 30°. Then we have $K^2\langle x^2 \rangle = (170/40)^2 = 18$ and $(170/110)^2 = 2.4$ at 90 and 30°, respectively; $g(\infty) = \exp(-K^2\langle x^2 \rangle)$ in models 3 and 4 is indeed very small. In addition to this, if we take into account a finite lifetime of the cage (i.e., $D_c > 0$ in model 4), the sideways translation of filaments, $D_1$, will be observed to be almost free by dynamic light scattering at not very low $\theta$ values. On the other hand, for $L_n = 90$ nm and $\langle cL^3 \rangle = 29$, we have $a_c = 17$ nm; sideways translation in this case will be observed to be strongly restricted even at the highest $\theta$, i.e., $D_1 \sim 0$ as in the model of Doi and Edwards [23]. Since many experiments have shown that the onset of semidilute regime appears in rotational diffusion at $cL^3 \sim 50$ [21,24,25], a major fraction of filaments with lengths up to about $L_w$ in a 0.5 mg/ml F-actin solution are expected to undergo almost free Brownian motion (fig. 6a). However, each of the very long filaments which contribute to the distant tail of $N(L)$ will be confined in several cages simultaneously, or in zig-zag tubing, with radius $a_c$ formed by a major fraction of filaments with lengths around $L_n$–$L_w$ (fig. 6b). If the filaments are rigid, any movement of very long filaments in such zig-zag tubing is not expected. Thus, motions of these filaments will be strongly restricted even if they are semiflexible. Lengthwise translation of a very long filament, $D_3$, will inevitably induce its forced bending. We can then expect a situation such as that in model 2; for simplicity, $D$ is assumed to express possible effects on $g(\tau)$ of the various modes of motion of a major fraction of filaments and $D_c$, those of restricted motions of very long filaments. If $D_c$ is very small, the first term on the right-hand side of eq. 10 signifies a very slowly decaying component

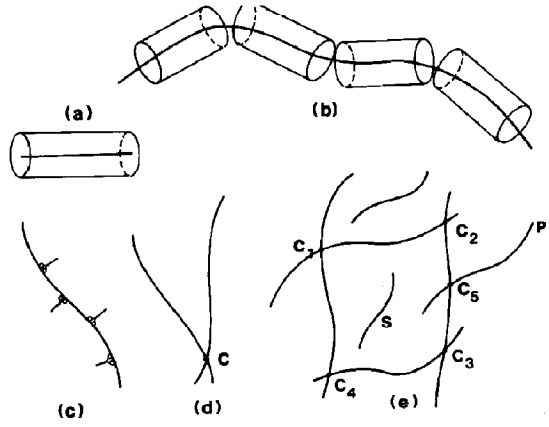


Fig. 6. Conceptual illustrations of entanglements of filaments. Semidilute solution of F-actin. (a) Test filament of length about $L_n$–$L_w$ confined in a cage formed by a major fraction of filaments where the test filament undergoes almost free Brownian motions. (b) Test filament of length several times greater than $L_n$ confined in cages, or zig-zag tubing, formed by a major fraction of filaments, where the test filament undergoes strongly restricted Brownian motions. Semidilute solution of acto-HMM. (c) Free filament decorated with HMMs. (d) Free filaments cross-linked (C) by HMM(s). (e) Network of filaments cross-linked by HMMs. $C_i$, P and S denote, respectively, cross-link, free end and free filament. Parts d and e: HMM decoration is not explicitly illustrated.

contributing to the $F$ values, and a very long time is needed to obtain $G^2(\tau)$ with high statistical accuracy [3].

For monodisperse bacteriophage fd, on the other hand, a time of 100–300 s/run was sufficiently long to obtain $G^2(\tau)$ at $cL^3$ up to 160 (or 6 mg/ml) and at $30° \leqq \theta \leqq 150°$ with very high statistical accuracy [7]. The lack of very long filaments in the bacteriophage fd preparation resulted in highly reproducible profiles even at low $\theta$ values and in a semidilute regime. Then, the question arises as to why the profiles for F-actin became reproducible at high $\theta$ values. This will be discussed below.

*4.2.3. $\bar{\Gamma}/K^2$ vs. $K^2$ relationships*

We shall first examine the effects of translational and rotational motions of filaments on $G^2(\tau)$. According to our theory for a rigid rod, the first cumulant $\bar{\Gamma}$ is given by [22,26]

$$\bar{\Gamma}/K^2 = D_0 + (L^2/12)\Theta f_1(k) + (D_3 - D_1)[f_2(k) - 1/3] \qquad (13)$$

where $D_0 = (2D_1 + D_3)/3$ is the overall translational diffusion coefficient, $D_1$ and $D_3$ the respective sideways and lengthways translational diffusion coefficients, $\Theta$ the end-over-end rotational diffusion coefficient, and $f_1(k)$ and $f_2(k)$, functions depending only on $k = KL/2$. In eq. 13, the second term on the right-hand side indicates the contribution from rotational diffusion and the third term that from anisotropy in translational diffusion. At $k \to 0$, we have $\bar{\Gamma}/K^2 \to D_0$. At finite $K^2$, $\bar{\Gamma}/K^2$ gives an apparent diffusion coefficient; at a given $K^2$, the larger the apparent diffusion coefficient, the greater is the involvement of the high-frequency modes of motion of the scatterer. For F-actin, we need to take account of an average of $\bar{\Gamma}/K^2$ over the length distribution $N(L)$;

$$\langle \bar{\Gamma}/K^2 \rangle_z = \int (\bar{\Gamma}/K^2) L^2 P(KL) N(L)\, dL \Big/ \int L^2 P(KL) N(L)\, dL \qquad (14)$$

where the subscript $z$ represents the so-called $z$-average and $P(KL)$ the scattering function. It is interesting to examine the limiting forms of $\langle D_0 \rangle_z$. For $D_0(L) = (k_B T/3\pi\eta L)[\ln(2L/d) - 0.73]$, which is the Broersma formula for $D_0$ without minor correction terms [27], it has been shown that

$$\langle D_0 \rangle_z = D_w(L_w) = (k_B T/3\pi\eta L_w) \times [\ln(2\alpha L_n/d) - 0.73] \quad (KL \to 0) \qquad (15)$$

$$= D_n(L_n) = (k_B T/3\pi\eta L_n) \times [\ln(2\alpha' L_n/d) - 0.73] \quad (KL \geqq 1) \qquad (16)$$

where $d$ is the rod diameter, $\alpha = 1.53$ and $\alpha' = 0.56$ for an exponential length distribution [9]. In the limit of $K^2 = 0$, $\langle D_0 \rangle_z$ is close to the Broersma value for $L = L_w$, although $\alpha L_n$ is smaller than $L_w$. On the other hand, for such long rods as F-actin at not very small $K^2$, $\langle D_0 \rangle_z$ is rather close to the Broersma value for $L = L_n$, although $\alpha'$ is smaller than unity.

The results obtained by machine computation of eq. 14 for the exponential length distribution with $L_n = 900$ nm [8,9] and $d = 8$ nm are shown in fig. 7. In the machine computation of eq. 14 with

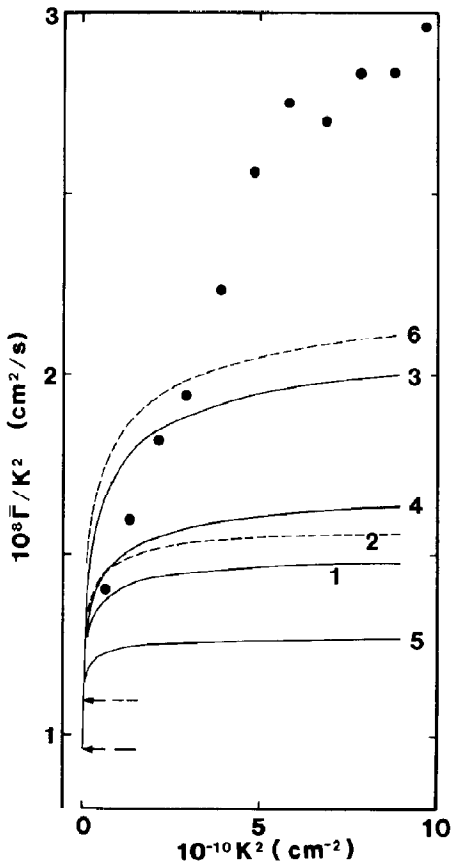


Fig. 7. Simulated results of $\langle \bar{\Gamma}/K^2 \rangle_z$ for rigid rods with an exponential length distribution (for details, see text) and experimental results (●) for F-actin taken from fig. 5. The number-average length was assumed to be $L_n = 900$ nm and solid curves were computed for $L \leqq 6000$ nm and dashed curves for $L \leqq 3500$ nm. Curves; (1, 2) $\langle D_0 \rangle_z$ vs. $K^2$ for dilute solution value of $D_0$; (3, 6) $\langle \bar{\Gamma}/K^2 \rangle_z$ vs. $K^2$ for dilute solution values of $D_i$ ($i = 0$, 1 and 3) and $\Theta$; (4) $\langle \bar{\Gamma}/K^2 \rangle_z$ vs. $K^2$ for dilute solution values of $D_i$ and one-half the dilute solution value of $\Theta$; (5) $\langle \bar{\Gamma}/K^2 \rangle_z$ for dilute solution values of $D_i$ and $\Theta = 0$. All solid curves begin at $K^2 = 0$ from the value indicated by the lower arrow, and dashed curves from that indicated by the upper arrow. (The difference between curves 3 and 5 gives $\langle (L^2/12)\Theta f_1(k) \rangle_z$, and the difference between curves 1 and 5 gives $-\langle (D_3 - D_1)[f_2(k) - 1/3] \rangle_z$.) The dilute solution values of $D_i$ and $\Theta$ were computed by use of Broersma's formulas. When compared with experimental results in a semidilute regime, it should be noted that these lines give an upper bound of $\langle \bar{\Gamma}/K^2 \rangle_z$ for each computational condition, because free translation was assumed for all rods including very long ones.

Broersma's formulas for $D(L)$ and $\Theta(L)$ including minor correction terms [27,28], the integration over $L$ was replaced by a summation up to $L = 6000$ nm with steps of 50 nm. For computation of $P(KL)$, the algorithms given in refs. 26 and 29 were used. Curve 1 in fig. 7 depicts the $\langle D_0 \rangle_z$ vs. $K^2$ relationship. This begins at $D_w(L_w)$ (indicated by the lower arrow) at $K^2 = 0$ and rapidly increases, reaching a plateau value of $D_n(L_n)$ as $K^2$ increases. Curve 2 shows the same relationship when the summation is truncated at $L = 3500$ nm. This commences at the value indicated by the upper arrow at $K^2 = 0$. The difference between these two curves arises from contributions to $\langle D_0 \rangle_z$ from very long filaments, although they amount to only 3% of the total. Curves 3–5 show $\langle \bar{\Gamma}/K^2 \rangle_z$ for $\Theta(L)$ of Broersma's value, for $\Theta$ of one-half of its dilute solution value and for $\Theta = 0$ respectively, and for $L \leqq 6000$ nm. (Curve 6 corresponds to curve 3 but for $L \leqq 3500$ nm.)

Since both $f_1(k)$ and $-[f_2(k) - 1/3]$ are increasing functions of $k$, the effects of polydispersity on the second and third terms in eq. 13 almost cancel out with each other [29], and the effect of polydispersity on $\langle \bar{\Gamma}/K^2 \rangle_z$ appears mostly through $\langle D_0 \rangle_z$ which is close to the number-average value except for very small $K^2$. Apart from the complexity due to the restricted motions of very long filaments at high $cL^3$, it is then suggested that complexity due to polydispersity can be mostly eliminated by adopting $L = L_n$ or an effective length $L_e$ which satisfies $D_0(L_e) = D_n(L_n)$, since $\langle D_0 \rangle_z$ (curve 1 in fig. 7) is nearly constant over the $K^2$ range we studied. The increase in observed values (●) at low $K^2$ is gradual compared with the $K^2$ dependence of curve 3. This is mostly due to a large contribution at low $K^2$ from a slowly decaying component(s) due to the restricted motions of very long filaments mentioned above. Note the sizes of the $F$ values in fig. 1. At high $K^2$, on the other hand, the observed values (●) exceed those of curve 3, although restricted motions of very long filaments more or less contribute to the spectrum. Hence, the excess values of the observed points over curve 3 (5) at high $K^2$ approximately give the lower (upper) bound of contributions to $\bar{\Gamma}/K^2$ from bending motions of filaments.

For a semiflexible filament, we have (cf. eq. 13)

$$\bar{\Gamma}/K^2 = D_0 + (L^2/12)\Theta f_1^*(k) + (D_3 - D_1)[f_2^*(k) - 1/3] + \sum_m D_{[m]} a_m(k) \qquad (17)$$

where $f_1^*(k)$, $f_2^*(k)$ and $a_m(k)$ ($m \geqq 2$) are functions of both $k$ and $\gamma$ (the flexibility parameter or the inverse of the Kuhn length) and $D_{[m]} = (k_B T/4\pi\eta L)(1 + f_m)$ ($m \geqq 2$) denotes the diffusion coefficient of the $m$-th mode of the bending motion [30,31]. The first three terms on the right-hand side of eq. 17 have the same meanings as those in eq. 13, and the last term(s) denotes the contribution(s) to $\bar{\Gamma}/K^2$ from the bending motion(s). In the stiff limit $\gamma \to 0$, $f_1^*(k) \to f_1(k)$, $f_2^*(k) \to f_2(k)$ and $a_m(k) \to 0$. The diffusion coefficients $D_0$, $D_1$, $D_3$ and $\Theta$ in eq. 17 are also functions of $\gamma$ (see, for example, refs. 9 and 32). The effect of nonzero $\gamma$ on the first three terms on the right in eq. 17 is indeed finite, but very small compared with that of polydispersity [32]. On the other hand, the last term(s) in eq. 17 has a large contribution(s) to $\bar{\Gamma}/K^2$. Since, however, various examples have been given in refs. 7, 9 and 30–33, we shall no longer discuss this problem.

Since the root-mean-square amplitude of the $m = 2$ bending mode ($< 60$ and 120 nm for $L = 1000$ and 2000 nm, respectively [9,32]) is smaller than the cage radius $a_c$, a major fraction of the filaments can also undergo almost free flexion motions (fig. 6a). Increased contributions at high $K^2$ from flexion motions of a major fraction of filaments, relative to the contribution from the restricted lengthwise translation of very long filaments, will result in highly reproducible profiles at high $K^2$. The amplitude $\langle x^2 \rangle$ in model 4 shows an analogy to the mean-square amplitude of the bending motion, so that even if $D_c$ is very small, increased contributions at high $K^2$ from various modes of restricted bending motions of very long filaments result in the faster decay of $g(\tau)$ in eq. 12 (note $g(\tau) \to \exp[-(D_c + D)K^2\tau]$ for large $K^2\langle x^2 \rangle$) and lesser values of $F$ at high $\theta$ in fig. 1.

### 4.3. Acto-HMM

#### 4.3.1. $\beta$ value

Carlson et al. [2,6] observed a very small $\beta$ value for acto-HMM, and interpreted their results on the basis of their formulation according to model 3 (their formulation is essentially the same as ours). They concluded that cross-linking of actin filaments by HMMs in the absence of ATP resulted in the gelation of filaments and decrease in $K^2\langle x^2\rangle$. In contrast to their results, ours given in ref. 3 and in figs. 2 and 3 included $\beta$ values as large as those of F-actin alone. As far as the $\beta$ value is concerned, our observations suggest either small $D_c$ in model 2, large $K^2\langle x^2\rangle$ in model 3, small $D_c$ and any size of $K^2\langle x^2\rangle$ in model 4, or any combination thereof. Small $D_c$ in model 2 would occur if HMM-binding could produce bundles of filaments without gelation. However, this case alone may be excluded since the solution did not pour from the inverted cell. Large $K^2\langle x^2\rangle$ in models 3 and 4 could be expected if acto-HMM gel was very soft; most of the HMMs bound to F-actin with two heads of each HMM on the same filament and cross-links by HMMs were sparsely distributed. Small $D_c$ (or slow movement of cross-links over a distance greater than $1/K$) in model 4 could be expected if the lifetime of cross-links was not infinite, and cycles of creation and annihilation of cross-links took place spontaneously.

The $\beta$ value was independent of the weight ratio up to 8 [3]. The $\bar{\Gamma}/K^2$ values at a given $K^2$ drastically decreased up to a weight ratio of unity but were virtually independent above unity (figs. 4 and 5). An acto-HMM solution of height 2 cm, for instance, did not pour from the inverted scattering cell without external disturbances such as mechanical shock being applied to it, whereas the same solution with a height of 7 cm did so without any external disturbance. In the latter case, the solution's own weight is expected to have induced its flow in the inverted cell. Acto-HMM solutions are highly thixotropic. Our results suggest that an acto-HMM gel is not rigid. However, it is difficult at present to visualize unequivocally an internal structure of an acto-HMM gel compatible with our observations.

In our experiments in 1979, we occasionally observed small $\beta$ values, viz., 0.1–0.15, for acto-HMM at 0.5, 1.0, 1.5 and 2.0 mg/ml F-actin and weight ratios of 1 and 2. Subsequently, we lifted the scattering cell slightly in the cell holder, and observed large $\beta$ values which varied from 0.5 to 0.7 run by run and from angle to angle at F-actin concentrations greater than or equal to 1 mg/ml. These $\beta$ values are comparable with that of about 0.7 for F-actin in that measurement. In the acto-HMM solution in that preparation, we observed visible inhomogeneity in the cell; some parts (not spots, but regions) in the solution scattered light more strongly than others. Model 1 and/or model 3 with small $K^2\langle x^2\rangle$ will account for these occasionally observed small $\beta$ values. We did not observe such visible inhomogeneity in both ref. 3 and this study. (Our statement, however, does not necessarily exclude other sources responsible for small $\beta$ values in acto-HMM, since the structure of acto-HMM is inferred to be strongly dependent on the steps and conditions of preparation. The visible inhomogeneity mentioned above might arise from a local variation in the cross-link density.)

#### 4.3.2. $\bar{\Gamma}/K^2$ vs. $K^2$ relationships

Although the motions of filaments slowed down on formation of rigor complexes, all the scattering elements were concluded as travelling distances far longer than $1/K$ because of large $\beta$ values. Fig. 6c–e depicts model situations for an acto-HMM gel. Decoration with HMMs (fig. 6c) decreases the diffusion coefficient of the filament. If filaments are cross-linked with each other by HMMs (fig. 6d), especially in a staggered fashion, the diffusion coefficient decreases greatly. In addition, when very long filaments are cross-linked by HMMs to form a network structure through the scattering cell, i.e., gel formation (fig. 6e), motions of not only cross-linked but also of free filaments in the network are strongly restricted. All of these sources and perhaps others are responsible for the decrease in $\bar{\Gamma}/K^2$ at any $K^2$ with weight ratio. Let us define the correlation function $g(\tau)$ of an acto-HMM system by

$$g(\tau) = i_{\text{free}} g_{\text{free}}(\tau) + i_{\text{gel}} g_{\text{gel}}(\tau) \qquad (18)$$

with $i_{free} + i_{gel} = 1$, where $g_{free}(\tau)$ conceptually expresses the correlation function for HMM-decorated filaments free from gelation and $g_{gel}(\tau)$ the correlation function for a gel. Then, $g_{free}(\tau)$ decays to zero at $\tau = \infty$ with a relatively high decay rate, although those free filaments undergo restricted motions in the network. $g_{gel}(\tau)$ will be given by $g(\tau)$ in model 3 or 4. Bending motions of cross-linked filaments will result in large values of $\langle x^2 \rangle$ and, at the same time, movement of cross-links over distances greater than $1/K$ (a temporal change in shape of the rhombus $C_1$-$C_2$-$C_3$-$C_4$ in fig. 6e, for example). Then, $g_{gel}(\tau)$ decays to practically zero at $\tau = \infty$, and a large $\beta$ value as well as a relatively high decay rate can be expected at high $K^2$. At low $K^2$, however, $K^2\langle x^2 \rangle$ may not be large enough to ensure large $\beta$ values. Spontaneous creation/annihilation of cross-links (and/or fragmentation/reannealing of filaments between cross-links) must be assumed in order to ensure nonzero $D_c$ in eq. 12. This very small $D_c$ will also be responsible for nonreproducibility of profiles at low $\theta$ values. If these model situations are assumed, then $\bar{\Gamma}/K^2$ vs. $K^2$ relationships can be qualitatively explained as follows. Slightly restricted rotational and bending motions of a major fraction of filaments, which are slightly decorated with HMMs, are mostly responsible for the increase in $\bar{\Gamma}/K^2$ with $K^2$ at a weight ratio of 0.5. On the other hand, in addition to the slightly restricted rotational and bending motions of relatively short filaments free from gelation (S in fig. 6e), 'segmental' motions of very long filaments cross-linked by HMMs are responsible for the increase in $\bar{\Gamma}/K^2$ with $K^2$ at weight ratios of unity and above. By segmental motion, we mean a bending motion of a filament either between two cross-links (e.g., $C_1$-$C_2$ in fig. 6e) or between its free end and the nearest cross-link (e.g., P-$C_5$ in fig. 6e). In order for such segmental motions to be able to contribute to a large excess $\bar{\Gamma}/K^2$ over that at $\theta = 30°$, acto-HMM must be more flexible than F-actin as we first suggested in ref. 1, because the segmental motion is restricted. There might be a number of filaments cross-linked in a staggered fashion, each of which does not necessarily consist of two filaments as depicted in fig. 6d, for example. Such a cross-linked filament will behave as if it were a single filament with greater flexibility than the truly single filament of the same length as that of the cross-linked filament. The population of these cross-linked filaments will also contribute to a large excess $\bar{\Gamma}/K^2$ at high $\theta$ values.

The decrease in $\bar{\Gamma}/K^2$ with weight ratios up to unity corresponds to the decrease in spectral width in $S^2(\omega)$; the narrowest width was observed at a weight ratio of unity [1]. Although no measurements were made here at weight ratios above 2, the previous study showed that $\bar{\Gamma}/K^2$ values at weight ratios of 4 and 8 were larger than those at weight ratios of 1 and 2 [3]. This also corresponds to our observation some time ago that the spectral width began to increase at weight ratios around 2 [1].

## 5. Concluding remarks

We would like to stress that for a given $cL^3$, say 30, the cage radius $a_c$ is quite large in long filaments; for $L = 1000$ nm, $a_c$ is larger than both $1/K$ (except for very low $\theta$ values) and the root-mean-square amplitude of bending motions. For instance, not only lengthwise but also sideways translational and bending motions of long filaments are almost free even at $cL^3 = 30$. An example of this situation will be given elsewhere with special reference to semidilute suspensions of monodisperse fd virus [33].

In the case of F-actin with exponential length distribution, very long filaments behave quite differently from the major fraction of filaments. The coexistence of a small number of very long filaments of length, say $5L$, with a large number ($cL^3 = 30$) of filaments with $L = 1000$ nm would mimic the present results for F-actin solution.

## References

1 S. Fujime and S. Ishiwata, J. Mol. Biol. 62 (1971) 251.
2 F.D. Carlson and A.B. Fraser, J. Mol. Biol. 89 (1974) 273.
3 S. Fujime, S. Ishiwata and T. Maeda, Biophys. Chem. 20 (1984) 1.

4 S. Fujime, in: Optical studies of muscle cross-bridge, eds. R. Baskin and Y. Yeh (CRC Press, FL, 1987) p. 149.
5 B. Chu, Laser light scattering (Academic Press, New York, 1974); B. Berne and R. Pecora, Dynamic light scattering (Interscience, New York, 1975).
6 A.B. Fraser, E. Eisenberg, W.W. Kielley and F.D. Carlson, Biochemistry 14 (1975) 2207.
7 T. Maeda and S. Fujime, Macromolecules 18 (1985) 2430; correction to typographical errors is in Macromolecules 19 (1986) 1494.
8 M. Kawamura and K. Maruyama, J. Biochem. (Tokyo) 67 (1970) 437.
9 J. Masai, S. Ishiwata and S. Fujime, Biophys. Chem. 25 (1986) 253.
10 F.B. Straub, Stud. Inst. Med. Chem. Univ. Szeged 3 (1943) 23.
11 S. Ebashi and K. Maruyama, J. Biochem. (Tokyo) 58 (1965) 20.
12 J.A. Spudich and S.J. Watt, J. Biol. Chem. 246 (1971) 4866.
13 A.G. Weeds and B. Pope, J. Mol. Biol. 111 (1977) 129.
14 A. Szent-Györgyi, Chemistry of muscular contraction, 2nd edn. (Academic Press, London, 1951).
15 S.H. Chen, W.B. Veldkamp and C.C. Lai, Rev. Sci. Instrum. 46 (1975) 1356.
16 D.E. Koppel, J. Chem. Phys. 57 (1972) 4814.
17 H.Z. Cummins, in: Photon correlation and light beating spectroscopy, eds. H.Z. Cummins and E.R. Pike (Plenum Press, New York, 1973), 225.
18 C. Kittel, Elementary statistical physics (John Wiley, New York, 1958).
19 R.W. James, The optical principles of the diffraction of X-rays (Bell and Sons, London, 1950).
20 K. Maruyama, M. Kaibara and E. Fukada, Biochim. Biophys. Acta 371 (1974) 20.
21 Y. Mori, N. Ookubo, R. Hayakawa and Y. Wada, J. Polym. Sci. Phys. 20 (1982) 2111.
22 T. Maeda and S. Fujime, Macromolecules 17 (1984) 1157.
23 M. Doi and S.F. Edwards, J. Chem. Soc. Faraday Trans. II 74 (1978) 560.
24 J.F. Maguire, J.P. McTague and F. Rondelez, Phys. Rev. Lett. 45 (1980) 1891; correction is in Phys. Rev. Lett. 47 (1981) 148.
25 K.M. Zero and R. Pecora, Macromolecules 15 (1982) 87.
26 S. Fujime and K. Kubota, Biophys. Chem. 23 (1985) 1.
27 S. Broersma, J. Chem. Phys. 32 (1960) 1632.
28 S. Broersma, J. Chem. Phys. 32 (1960) 1620.
29 K. Kubota, Y. Tominaga, S. Fujime, J. Otomo and A. Ikegami, Biophys. Chem. 23 (1985) 15.
30 T. Maeda and S. Fujime, Macromolecules 17 (1984) 2381.
31 S. Fujime and T. Maeda, Macromolecules 18 (1985) 191.
32 S. Sasaki and S. Fujime, Biophys. J. 51 (1987) 503.
33 S. Fujime, M. Takasaki-Ohsita and T. Maeda, Macromolecules 20 (1987) 1292.